JACS
JOURNAL OF THE AMERICAN CHEMICAL SOCIETY
Article
pubs.acs.org/JACS

Ligand Field Effect at Oxide–Metal Interface on the Chemical Reactivity of Ultrathin Oxide Film Surface

Jaehoon Jung,[†,‡] Hyung-Joon Shin,[§] Yousoo Kim,*[,†] and Maki Kawai*[,‡]

[†]RIKEN Advanced Science Institute, 2-1 Hirosawa, Wako, Saitama 351-0198, Japan

[‡]Department of Advanced Materials Science, The University of Tokyo, 5-1-5 Kashiwanoha, Kashiwa, Chiba 277-8561, Japan

[§]School of Mechanical and Advanced Materials Engineering and Low Dimensional Carbon Materials Center, Ulsan National Institute of Science and Technology (UNIST), 100 Banyeon-ri, Eonyang, Ulju-gun, Ulsan 689-798, Republic of Korea

Supporting Information

ABSTRACT: Ultrathin oxide film is currently one of the paramount candidates for a heterogeneous catalyst because it provides an additional dimension, i.e., film thickness, to control chemical reactivity. Here, we demonstrate that the chemical reactivity of ultrathin MgO film grown on Ag(100) substrate for the dissociation of individual water molecules can be systematically controlled by interface dopants over the film thickness. Density functional theory calculations revealed that adhesion at the oxide–metal interface can be addressed by the ligand field effect and is linearly correlated with the chemical reactivity of the oxide film. In addition, our results indicate that the concentration of dopant at the interface can be controlled by tuning the *drawing effect* of oxide film. Our study provides not only profound insight into chemical reactivity control of ultrathin oxide film supported by a metal substrate but also an impetus for investigating ultrathin oxide films for a wider range of applications.

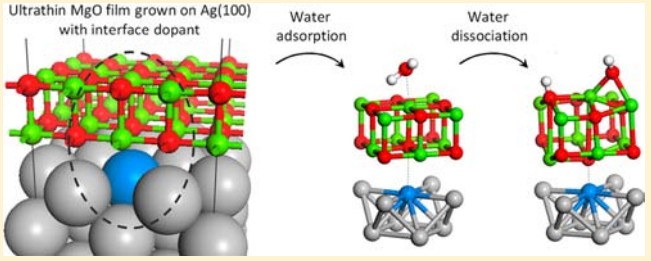

INTRODUCTION

A variety of oxides have long been considered potential materials for applications ranging from gas sensing, coating, and catalysts to use as magnetic, optical, and electronic devices due to their diverse chemical and physical properties.[1] The fundamental importance of and great interest in oxide materials have been extended of late to their ultrathin films because they provide an additional controllable dimension, that is, film thickness, which is not available in bulk oxides.[2,3] In particular, ultrathin oxide films, such as MgO, Al_2O_3, FeO, and SiO_2, grown on metal substrates have been intensively investigated not only as supporting materials for chemically active nanoparticles but also as catalysts.[4,5] Typical ways to control the properties of adsorbates on ultrathin oxide films via various tunable factors are illustrated in Figure 1: (1) charge redistribution between adsorbates and the oxide–metal interface is considered significant in activating adsorbates, such as O_2, NO_2, and Au atoms or clusters, which can be described by both workfunction reduction due to oxide film and high electron affinity (EA) of adsorbates;[6−11] (2) the enhancement of adhesion strength with strong polaronic distortion plays a pivotal role in H_2O dissociation on MgO/Ag(100);[12−14] (3) the thickness of the oxide film closely associates with both the charging of adsorbates and interface adhesion;[11−13,15] last, (4) the change in oxygen composition of polar FeO film grown on Pt(111) was reported to facilitate CO oxidation depending on the ambient oxygen concentration.[16,17]

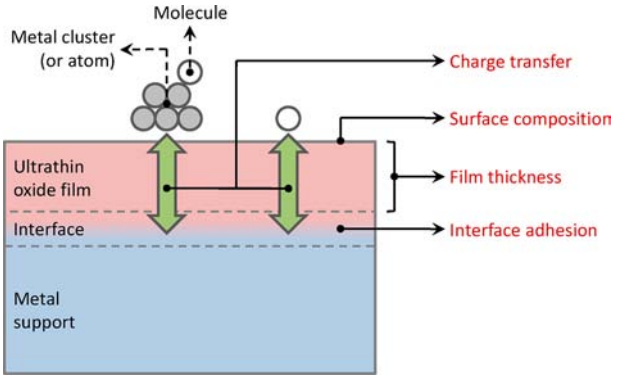

Figure 1. Schematic diagram of the factors having an influence on the chemical reactivity of ultrathin oxide film supported by a metal substrate.

Remarkable controllability in the chemical reactivity of an ultrathin oxide film compared to its bulk counterpart has been found in water dissociation on ultrathin MgO film supported by a Ag(100) substrate,[13,15,18] which is a subject not only of an increasing level of attention as an elementary step for pure hydrogen generation[19] but also of fundamental scientific interest.[20] Water dissociation on ultrathin MgO film has been reported to be largely enhanced compared to that on the bulk

Received: March 27, 2012
Published: May 25, 2012

dx.doi.org/10.1021/ja302949j | J. Am. Chem. Soc. 2012, 134, 10554−10561

via experiments using X-ray photoelectron and Auger spectroscopic methods.[18] As well, we have recently demonstrated, using scanning tunneling microscopy experiment combined with density functional theory (DFT) calculations, that the dissociation path of individual water molecules ($H_2O \rightarrow 2H^+ + O^{2-}$ or $OH^- + H^+$) on MgO/Ag(100) can be selectively achieved by varying the energy of tunneling electrons and that the chemical reactivity of ultrathin MgO film can be controlled by the film thickness.[15] We revealed that the change in adhesion strength due to the electronic structure at the oxide−metal interface is essential to explaining the film thickness dependence of chemical reactivity for water dissociation, which is not influenced by the charging of adsorbates on the film surface, due to the low EA of adsorbates during the reaction.[13] In addition to water dissociation, the oxide−metal interface also plays an important role in the dissociation of O_2 molecules on MgO/Ag(100), where O_2 molecules with high EA are activated by the charge transfer from the interface, and thus it has been theoretically suggested as a low-temperature CO oxidation catalyst.[9,10] Therefore, we have recently proposed that manipulation of the local interface structure, for example, introducing an oxygen vacancy at the interface, can be applied to enable tailoring of the chemical reactivity of the ultrathin oxide film.[14]

Surface engineering techniques such as ad-atoms, doping, and alloys have been considered promising solutions for creating surfaces with desired chemical and physical properties.[21−23] However, studies on interface engineering of ultrathin oxide films grown on metal substrates are yet rarely performed and demand a more systematic approach to get deep insight.[14,24] Interface engineering can be suggested as a strategy for improving durability because the interface is protected from chemical reactions occurring on the surface. Here, using spin-polarized periodic DFT calculations, we demonstrate that the chemical reactivity of an ultrathin MgO film supported by a Ag substrate can be systematically controlled with an interface dopant and further accounted for, with the aid of ligand field theory (LFT),[25] by the interaction between the dopant and the oxide layer at the interface. As model systems for interface engineering, we introduced to the oxide−metal interface 3d transition metal (TM) dopants (D_{TM} = Sc ∼ Zn) (Figure 2) that have been successfully used in controlling photocatalytic[26]

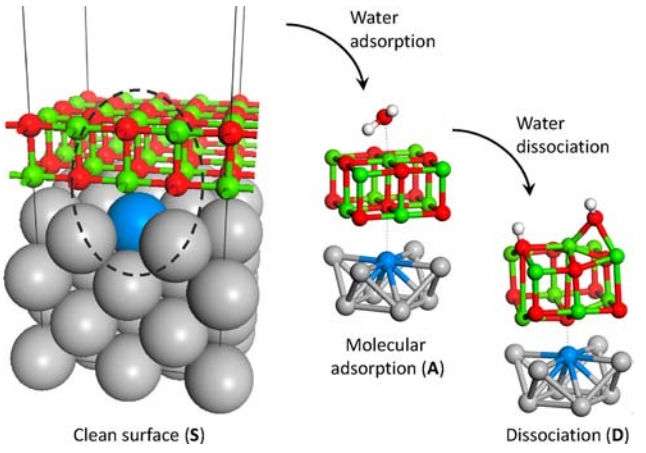

Figure 2. Dissociation of water molecules on ultrathin MgO film grown on Ag(100) substrate with interface dopants of first row 3d transition metal. (Ag, gray; 3d TM dopant, blue; Mg, green; O, red; H, white)

and magnetic[27] behaviors of oxide materials due to the high tunability with a number of d electrons. Introduction of dopants[28,29] or interstitials[30] at subsurface layers of the oxide support has also been demonstrated as a way to tailor the equilibrium shape of gold ad-particles and thus chemical reactivity.

RESULTS AND DISCUSSION

Stability of Dopants at the Oxide−Metal Interface. Whereas the modification of chemical composition with dopants permits the control of material functions, it may also cause instability issues due to structural distortion.[31] Therefore, we first evaluated the thermodynamic stability of the interface dopant via formation energy calculations at a single impurity level. Part a of Figure 3 shows the formation energies associated with doping, that is, the substitution of 3d TM atoms (Sc ∼ Zn) onto the first Ag layer of both bare and MgO film-covered Ag(100) substrates, $E^{dop}_{f(1)}$(Ag(100)) and $E^{dop}_{f(1)}$(MgO/Ag(100)), respectively. For all elements except Zn, the substitution of a Ag atom by a 3d TM atom is thermodynamically favorable both at the surface layer of Ag(100) and at the interface Ag layer of MgO/Ag(100). The energy difference ($\Delta E^{dop}_{f(1)}$) between $E^{dop}_{f(1)}$(MgO/Ag(100)) and $E^{dop}_{f(1)}$(Ag(100)) shows that the MgO film stabilizes the interface dopant and the amount of stabilization decreases overall when going up in the 3d series from Ti to Zn (filled circles in part c of Figure 3 and also Table S1 of the Supporting Information for detailed numerical values). This qualitatively agrees well with the bond energy descriptor for the TM−O interaction in 3d TM oxides,[32] which implies that, as the interaction between oxygen and TM dopant at the interface strengthens, the more effectively the dopant is stabilized.

The chemical composition at the surface region of an alloy system may differ from that at the bulk region,[33] because the dopants can migrate to the interior of the bulk layer as observed in Pd/Ag(100).[34] Therefore, we investigated the spatial preference of a dopant in (oxide film-covered) metal substrate with the energy difference according to the location of the dopant in the host metal substrate. Part b of Figure 3 shows the difference between the formation energies for doping into the first and second layers of a Ag substrate for both bare and MgO film-covered Ag(100), $\Delta E^{dop}_{f(1-2)}$(Ag(100)) and $\Delta E^{dop}_{f(1-2)}$(MgO/Ag(100)), respectively. It is obvious that the TM dopant can be remarkably well stabilized at the MgO−Ag interface in comparison with the uncovered Ag(100) surface (as indicated by the dotted arrow in part b of Figure 3). This spatial preference of the dopant indicates that the deposition of oxide film can enhance the concentration of the dopant at the interface layer of MgO/Ag(100). The amount of stabilization of the interface dopant due to MgO film with respect to when the dopant locates at the second layer of the Ag substrate, $\Delta\Delta E^{dop}_{f(1-2)}$, is similar to $\Delta E^{dop}_{f(1)}$ as a matter of course, because the stability of interface dopant increases as the TM−O interaction strengthens (open circles in part c of Figure 3). As a result, from the thermodynamic viewpoint, the Ti and Sc dopants are expected to be dominantly positioned at the oxide−metal interface. Our results imply not only that the deposition of ultrathin oxide film on the metal substrate including dopants promises to achieve desired imperfections at the oxide−metal interface, which we term the *drawing effect* of oxide film, but also that the relative distribution of dopants at the oxide−metal interface can be predicted using the interaction strength between (anionic) oxygen and TM dopants.

dx.doi.org/10.1021/ja302949j | J. Am. Chem. Soc. 2012, 134, 10554−10561

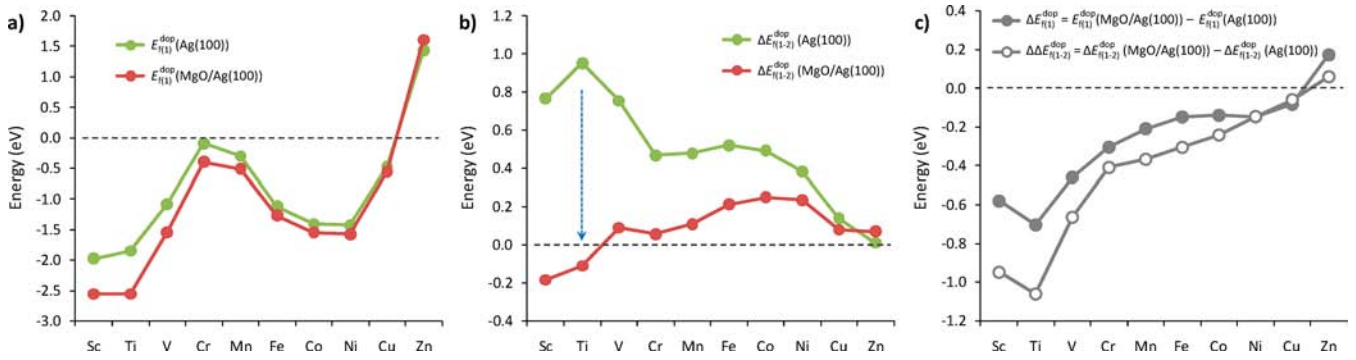

Figure 3. Stability of dopants at the oxide−metal interface. (a) Formation energies due to doping of 3d TM atom to first layer of both bare and MgO-covered Ag(100) substrates, $E^{dop}_{f(1)}$(Ag(100)) and $E^{dop}_{f(1)}$(MgO/Ag(100)), respectively. (b) The difference between the formation energies for doping at the first and second layers in a Ag substrate of Ag(100) and MgO/Ag(100), $\Delta E^{dop}_{f(1-2)}$(Ag(100)) and $\Delta E^{dop}_{f(1-2)}$(MgO/Ag(100)), respectively. The increase of stabilization due to the *drawing effect* of MgO film is indicated by dotted arrow. The minus (plus) sign in energy indicates that the preference position of dopant is first (second) layer. (c) The amounts of stabilization of the dopant at the interface layer due to MgO film for (a) and (b), $\Delta E^{dop}_{f(1)}$ and $\Delta\Delta E^{dop}_{f(1-2)}$, respectively.

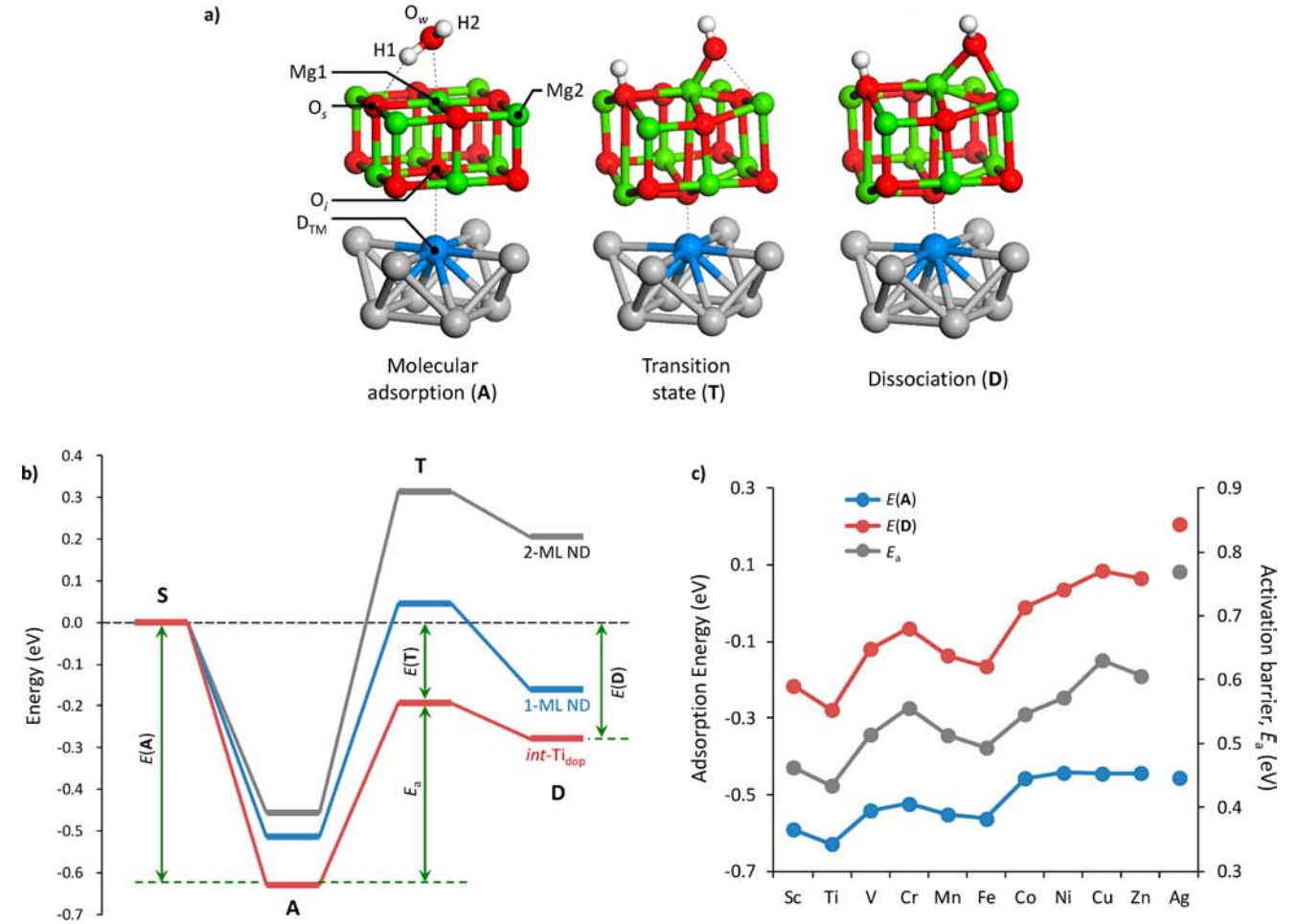

Figure 4. Water dissociation on MgO/Ag(100) with interface dopants. (a) Dissociation mechanism of the individual water molecule on an ultrathin MgO film supported by doped and nondoped Ag(100) substrates. (Ag, gray; 3d TM dopant, blue; Mg, green; O, red; H, white) (b) Reaction energy diagram (in eV) for the water dissociation on the nondoped (ND) 1- and 2-ML MgO/Ag(100) surfaces and on MgO film surface deposited on a Ti-doped Ag(100) substrate (*int*-Ti_{dop}) at the oxide−metal interface. Nondissociative adsorption (**A**), transition state (**T**), and dissociative adsorption (**D**) energies are evaluated relative to $E(H_2O) + E$(Substrate) = 0 eV. Dissociation barrier, $E_a = E(\mathbf{T}) - E(\mathbf{A})$. (c) The variations of $E(\mathbf{A})$, $E(\mathbf{D})$, and E_a along the 3d TM (Sc ∼ Zn) dopants.

Dissociation of Water Molecules on MgO/Ag(100) with an Interface Dopant. To investigate the influence of interface dopant on the chemical reactivity of ultrathin oxide film for the dissociation of water molecules, we examined the dissociation mechanism of individual water molecules adsorbed upon a MgO film surface with a dopant as shown in part a of Figure 4. A water molecule first adsorbs asymmetrically on top of the surface magnesium (Mg1), located over a TM dopant

dx.doi.org/10.1021/ja302949j | *J. Am. Chem. Soc.* 2012, 134, 10554−10561

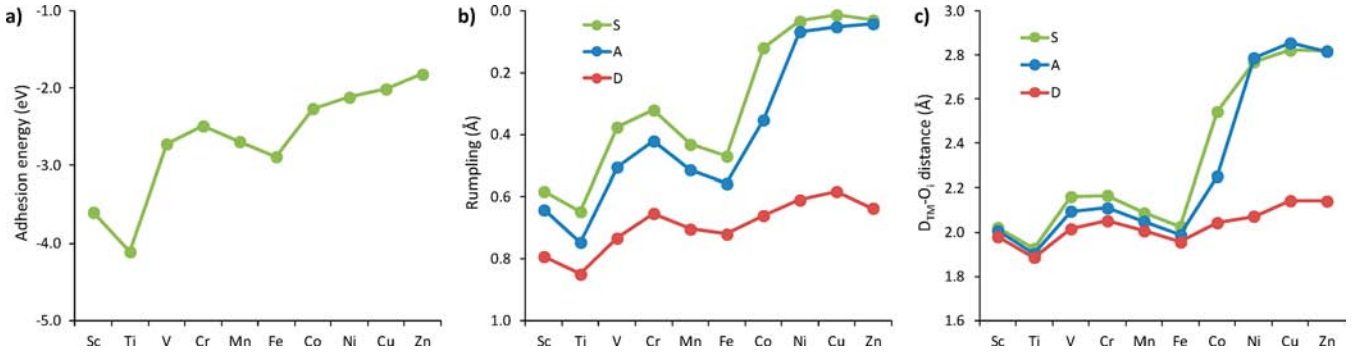

Figure 5. Double-humped pattern in the adhesion properties of the interface doped MgO/Ag(100). The variations of (a) adhesion energy between oxide and metal layers, (b) rumpling of interface MgO layer, and (c) D_{TM}-O_i distance during water dissociation, from before adsorption (**S**) through molecular adsorption (**A**) to the dissociative adsorption (**D**) stages, on doped MgO/Ag(100). The adhesion energy, $E_{adh} = E(int\text{-}M_{dop}) - [E(MgO) + E(M\text{-doped Ag})]$, is calculated using the corresponding geometry in the optimized structure for **S** stage. The rumpling is defined as the difference between the z coordinates of the highest and lowest atoms in the layer. The atomic notations are marked in part a of Figure 4.

(D_{TM}), where one hydrogen atom (H1) interacts with a neighboring surface oxygen (O_s) via hydrogen bonding. When the water molecule dissociates into $H^+ + OH^-$, H^+ forms a hydroxyl ion (O_sH1) by bonding with surface oxygen, and OH^- (O_wH2) bonds with the two nearest magnesium ions (Mg1 and Mg2). (w and s denote water and surface, respectively.) It should be noted that the dissociation mechanism is not changed by the interface dopants compared with the nondoped system, which means that the chemical reactivity of the MgO film grown on a Ag(100) substrate can be controlled by interface manipulation with the established mechanism.[12,13,15] Part b of Figure 4 shows the reaction energy diagram for the dissociation of individual water molecules on nondoped (ND) 1- and 2-ML MgO/Ag(100) surfaces[13,15] and on an MgO film surface deposited on a Ti-doped Ag substrate (*int*-Ti_{dop}), where Ti is the most reactive dopant among all the 3d TM series (part c of Figure 4 and Table S2 of the Supporting Information for detailed numerical values). All energies are evaluated relative to $E(H_2O) + E(\text{substrate}) = 0$ eV, that is, the clean surface before adsorption (**S**). A remarkable improvement in chemical reactivity for water dissociation over thickness dependence[13,15] was achieved in *int*-Ti_{dop}, where the water molecule is more strongly adsorbed and more easily dissociated on *int*-Ti_{dop}. The nondissociative molecular adsorption ($E(\mathbf{A})$), transition state ($E(\mathbf{T})$), and dissociative adsorption ($E(\mathbf{D})$) energies for *int*-Ti_{dop} are lower than those of ND film with same film thickness by 0.17, 0.51, and 0.48 eV, respectively. The barrier height (E_a), $E(\mathbf{T}) - E(\mathbf{A})$, is, therefore, noticeably reduced by 44% and 60% from those of 2-ML ND MgO film and bulk MgO, respectively. We have already reported such improvement in the chemical reactivity of MgO/Ag(100) for water dissociation by an O vacancy at the interface MgO layer[14] (Table S2 of the Supporting Information). However, the formation energy for an interface dopant (e.g., −2.55 eV for *int*-Ti_{dop}) is much lower than that for O vacancy formation (5.30 eV for *int*-O_{vac}) at the oxide−metal interface. This result indicates that the interface dopants with 3d TM provide a better chance for controlling the chemical reactivity of ultrathin oxide film than expected with the interface O vacancy.

Our systematic study on the doping of 3d TM into the oxide−metal interface provides a new perspective that the chemical reactivity of ultrathin oxide film grown on a metal substrate can be finely tuned by interface manipulation. Part c of Figure 4 shows the variation of the reaction energies, such as $E(\mathbf{A})$, $E(\mathbf{D})$, and E_a, during the dissociation of individual water molecules on MgO/Ag(100) according to the kind of interface dopant (Sc ∼ Zn). Interestingly, the shape of reaction energy variation along 3d TM series clearly shows a *double-humped pattern*,[35] which is commonly observed in organometallic systems explained by ligand field stabilization energy (LFSE) with weak field ligands (Figure S1 of the Supporting Information for the magnetic moments and the atomic charges of interface dopants). The electronic configuration of high-spin TM complexes represented by the small ligand field splitting of TM d orbitals results in a characteristic double-humped pattern according to the amount of d electron stabilization such as the hydration enthalpy of bivalent TM ions ($[TM(H_2O)_6]^{2+}$).[36] Because the only compositional difference among the systems is a TM dopant introduced into the interfacial metal layer, the result illustrated in part c of Figure 4 reasonably suggests that interfacial $D_{TM}-O_i$ interaction is closely related to the chemical reactivity of ultrathin MgO film. All representative adhesion properties (Figure 5) reinforce the ligand field effect (i.e., $D_{TM}-O_i$ interaction) at the oxide−metal interface, in which all the properties present the double-humped pattern with the identical minima (Ti and Fe) as shown in part c of Figure 4. The more reactive TM-doped system accompanies the larger adhesion energy (part a of Figure 5), the stronger rumpling (part b of Figure 5) and the shorter distance between dopant and interacting oxygen ($d(D_{TM}-O_i)$) (part c of Figure 5). Our result is consistent with the importance of local geometric and electronic structures due to interface dopant in determining the global adhesion of Al_2O_3/Ni(111).[37] The much larger change in the double-humped pattern at the higher 3d series (Co ∼ Zn), as shown in parts b and c of Figure 5, can be also explained by a greater change in adhesion strength compared to those of lower 3d series during the dissociation of adsorbed water molecules (**A** → **D**). As we already reported in a previous study of *int*-O_{vac},[14] the enhancement of the charge density accumulation at the interface can address the stronger adhesion strengthening at the higher 3d series during dissociation (**A** → **D**) compared to the nondissociative molecular adsorption (**S** → **A**). (charge density difference maps in Figures S2−S4 of the Supporting Information.)

Ligand Field Effect for a Dopant at the Oxide−Metal Interface. The nature of the interfacial interaction between oxide film and a metal substrate cannot be easily described by a single term because it consists of complex combinations of various contributing factors: hybridization, polarization, charge

dx.doi.org/10.1021/ja302949j | *J. Am. Chem. Soc.* 2012, 134, 10554−10561

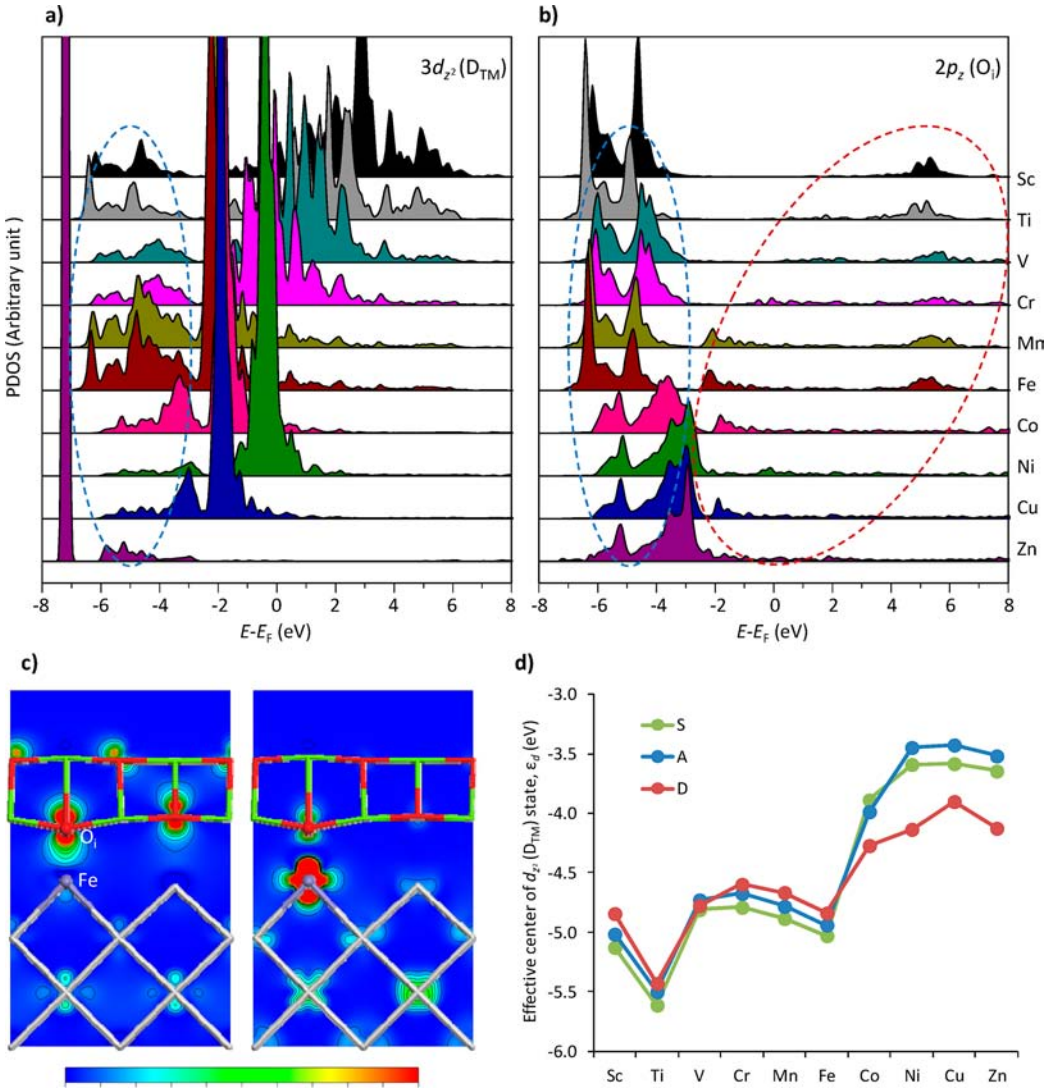

Figure 6. Electronic structure at the interface determined by ligand field effect. Projected density of states (PDOS) of 3d TM (D_{TM}) doped MgO/Ag(100) (*int*-M_{dop}, M = Sc ∼ Zn) before the adsorption of water molecule (**S**); (a) $3d_{z^2}(D_{TM})$ and (b) $2p_z(O_i)$. The scale in the *y* axis is (a):(b) = 2:1. Only up-spin states are plotted for clarity considering the weak field nature (Figure S1 of the Supporting Information). Bonding and antibonding states are depicted in (a) and (b) with blue and red dotted lines, respectively. (c) Band-decomposed partial charge density maps (at Γ-point) corresponding to the bonding (left, −6.24 eV) and antibonding (right, −1.65 eV) states between $3d_{z^2}$(Fe) and $2p_z(O_i)$ in occupied region of *int*-Fe_{dop} system. Color and contour grid for the probability of finding the electron varies from 0.00 (blue) to 0.01 (red) *e*/bohr.^{3} (d) The variation of the effective center of occupied $2p_z(O_i)$ states (ε_d) as an indicator of the splitting order of $3d_{z^2}$ states of the TM dopant, from before adsorption (**S**) through molecular adsorption (**A**) to the dissociative adsorption (**D**) stages, on *int*-M_{dop} (M = Sc ∼ Zn). The ε_d values are evaluated in the occupied region within 8 eV from Fermi level (E_F).

transfer, dispersion, and so forth.[4,38,39] Despite those complexities, we show that the chemical reactivity of an ultrathin oxide film supported by a doped-metal substrate can be mainly governed by the hybridization between the electronic states of a D_{TM} and an O_i (of oxide layer) at the interface. For systematic study on the influence of dopants upon the electronic structure at the oxide−metal interface, the projected density of states (PDOS) diagrams of $3d_{z^2}(D_{TM})$ and $2p_z(O_i)$ states for the all doped MgO/Ag(100) systems are illustrated in parts a and b of Figure 6, respectively. The distribution of electronic states for bonding and antibonding states is depicted by dotted blue and red circles respectively on the PDOS diagram of $2p_z(O_i)$ states (parts a and b of Figure 6). The identical alignment of the bonding states (about −7 ∼ −3 eV) between a D_{TM} and an O_i in PDOS diagrams indicates the existence of orbital interaction along the *z* axis at the interface. Part c of Figure 6 clearly shows the charge density distribution of the bonding and antibonding states between $3d_{z^2}(D_{TM})$ and $2p_z(O_i)$ states in the occupied region for *int*-Fe_{dop}, which corresponds to the second minimum of the double-humped pattern shown in part c of Figure 4. Hybridization, that is, the formation of bonding and antibonding states, between the electronic states of D_{TM} and O_i indicates that ultrathin MgO film behaves as a ligand for the interface dopants. (Figure S5 of the Supporting Information for the detailed PDOS diagrams of *int*-Ti_{dop} and *int*-Fe_{dop} during the reaction.) The correlation between global adhesion strength and the local D_{TM}−O_i interaction is also well explained by the PDOS diagrams. At the higher 3d series (Mn ∼ Zn), the antibonding states become partially occupied (about −2 ∼ 0 eV) and their adhesion energies decrease overall compared to the lower 3d series, as shown in part a of Figure 5. For quantitative discussion on the correlation between the adhesion

energy, or further chemical reactivity, of the interface-doped MgO/Ag(100) and the d states arrangement at the interface, we employed the effective center of occupied $2p_z(O_i)$ states (ε_d) as an indicator of the splitting order of $3d_{z^2}(D_{TM})$ states (part d of Figure 6). The electronic structure of $3d_{z^2}$ states of dopants also involves interaction with the Ag substrate, as well as with the interfacial oxygen (O_i) of MgO, and thus is too complicated to be used in the analysis as shown in part a of Figure 6. Therefore, the strongly localized $2p_z(O_i)$, only hybridized with interface dopants, was used to evaluate the amount of d states splitting due to $D_{TM}-O_i$ interaction along the z axis. The ε_d was evaluated in the occupied region from −8 eV to the Fermi level (E_F), in which the weakening effect due to the occupation of antibonding states can be counted as well as the alignment of electronic states due to ligand field effect at the interface.[40] The variation of ε_d shows a very similar pattern to that of adhesion strength (part a of Figure 5) and further chemical reactivity (part c of Figure 4) depending on the kind of dopants.

Finally, we examined for correlation among adhesion energy, chemical reactivity and the electronic structure at the interface in detail. Part a of Figure 7 clarifies that the amount of splitting in D_{TM} d states due to hybridization between the electronic states of the dopants (TM) and MgO film (ligand) can be considered a dominant factor in determining the chemical reactivity of the interface-doped MgO/Ag(100). The linear regression results presented in part b of Figure 7 also show a remarkable correlation between the chemical reactivity of ultrathin MgO film and adhesion energy between MgO and Ag layers. It should here be stressed that the electronic structure and adhesion energy of a clean MgO/Ag(100) before adsorption (**S**) has good correlation with $E(\mathbf{A})$, even further with $E(\mathbf{D})$ and E_a. Thus, the splitting in D_{TM} d states by ligand field effect at the interface can be considered as a promising descriptor in estimating chemical reactivity for efficient materials design.

Our results revealed that the chemical reactivity of the oxide film surface is strongly dependent on the tailored electronic structure caused by the interface dopants at the impurity level, which implies that chemical reactivity can be systematically controlled by adjusting adhesion strength using interface dopants. This observation strongly suggests the advantage of interface manipulation compared to direct modification of a surface structure. The manipulated interface can be protected from chemical reactions by ultrathin oxide film. Therefore, the durability of the developed system and the fine-tuning of its chemical reactivity can be achieved without serious perturbation in the reaction mechanism. In addition, the variation of adhesion energy depending on the kind of dopant originates from hybridization between the electronic states of the interface dopants (D_{TM}) and interface oxygen (O_i), that is, TM−ligand interaction, which can be described by traditional LFT, despite the complexity, such as the symmetry of ligand field and the charge state of TM, compared to simple organometallic systems.

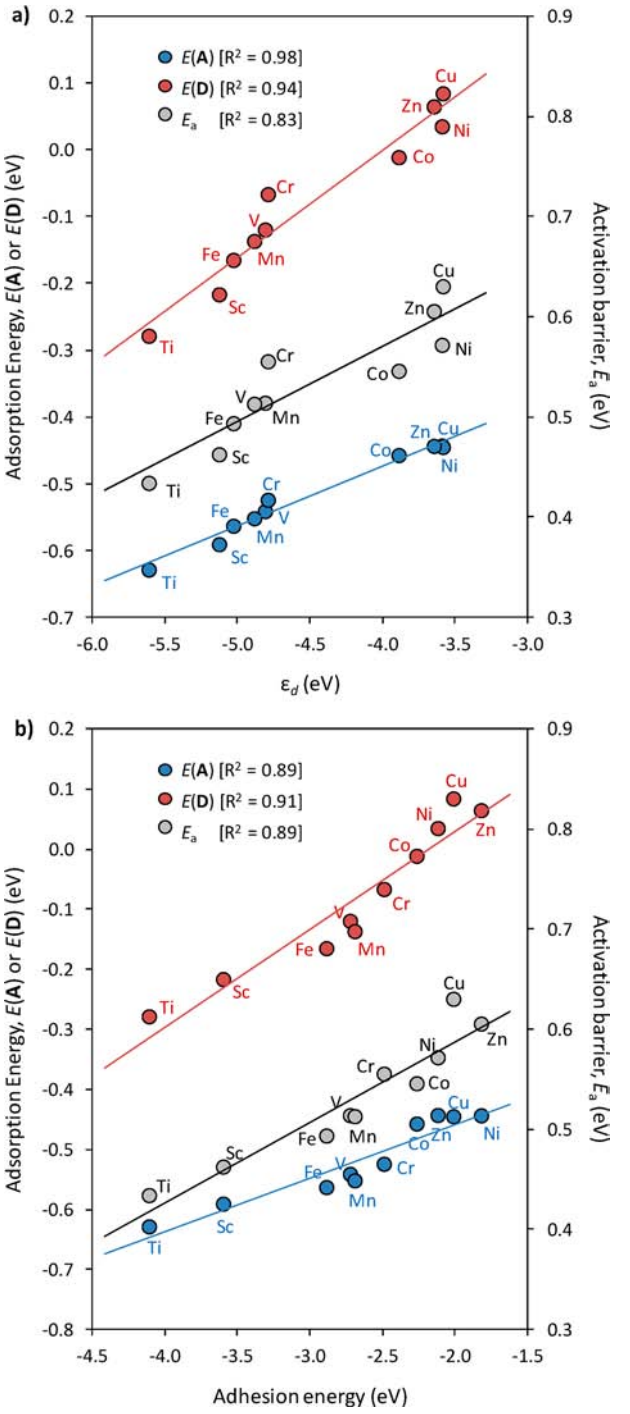

Figure 7. Ligand field effect on the chemical reactivity of ultrathin oxide film. The correlation of the chemical reactivity of 3d TM (D_{TM}) doped MgO/Ag(100) (*int*-M_{dop}, M = Sc ~ Zn) with (a) the order of d state splitting (ε_d) and with (b) the adhesion energy. The ε_d and adhesion energy are evaluated with respect to the geometric and electronic structures before molecular adsorption (**S**). The R^2 values of simple linear regression analysis are presented at each corresponding graph.

CONCLUSIONS

The influence of a comprehensive series of 3d TM dopants on the chemical reactivity of ultrathin MgO thin film grown on a doped Ag substrate was investigated using periodic DFT calculations. Our study reveals that TM dopants can be effectively stabilized by an oxide film, which suggests not only that the deposition of ultrathin oxide film is a promising way to enhance the concentration of dopants at the interface by the *drawing effect* of oxide film but also that the concentration of dopants at the oxide−metal interface depending on the kind of dopant is quite predictable using the relative oxygen affinity of TM dopants. The chemical reactivity of ultrathin MgO films supported by a Ag(100) substrate can be enhanced by

dx.doi.org/10.1021/ja302949j | J. Am. Chem. Soc. 2012, 134, 10554−10561

introducing interface dopants in a controlled manner. The double-humped pattern in chemical reactivity of ultrathin oxide film depending on the dopant can be explained by the variation in adhesion energy, which reflects the amount of local hybridization between the electronic states of the TM dopant and oxide film, that is, ligand field effect, at the interface. The amount of d state splitting of the TM dopant caused by the ligand field formed by the oxide film fully correlates to the pattern of chemical reactivity change. Therefore, our results provide strong impetus for introducing and characterizing interface irregularity from the atomic-scale insights accumulated thereby. Such challenges could result in a significant ripple effect on the development not only of heterogeneous catalyst but also of novel potential materials, in which the interface plays a pivotal role in determining the function of materials, such as the electronic and magnetic conductivity of complex oxide materials[41] and the tunneling barrier of magnetic tunneling junction systems.[42]

COMPUTATION DETAILS

Spin-polarized periodic density functional calculations were performed using the Vienna ab initio Simulation Package (VASP) code[43,44] with the Perdew–Wang exchange-correlation functional (PW91).[45,46] Core electrons were replaced by projector-augmented wave (PAW) pseudopotentials,[47] expanded in a basis set of plane waves up to a cutoff energy of 400 eV. To focus on the isolated single molecule without intermolecular interaction among neighboring adsorbates on the surfaces, we used $(2\sqrt{2} \times 2\sqrt{2})R45°$ surface supercells corresponding to $^1/_8$ ML H_2O molecules on the 2-ML MgO/Ag(100) surface with or without an impurity dopant, 3d TM atom (Sc ∼ Zn), on a Ag substrate. The calculated lattice constants are 4.15 and 4.20 Å for Ag and MgO respectively, which agrees with other theoretical and experimental values to within ∼2%.[48] The slab models consist of two layers of MgO and four layers of Ag. The periodically replicated slabs were separated by a vacuum region of ∼15 Å. During ionic relaxations, the two bottom Ag layers were fixed in their bulk positions. Ionic relaxations were performed until atomic forces were less than 0.01 eV/Å. $2 \times 2 \times 1$ and $6 \times 6 \times 1$ Γ-centered grids were used for the *k*-point sampling of the Brillouin zone for ionic relaxation and various analyses such as Bader population[49] and electronic density of states (DOS), respectively. The transition states for water dissociation were obtained using the climbing image nudged elastic band (CI-NEB) method[50] and confirmed by vibrational frequency calculations. Dipole correction was applied in order to avoid interactions between periodic slab images. All calculations were performed without any symmetry restrictions.

To quantitatively analyze the correlation between the interface electronic structure and adhesion energy, or further chemical reactivity of doped MgO/Ag(100), we employed the effective center of occupied $2p_z(O_i)$ states (ε_d) as an indicator of the splitting order of $3d_{z^2}(D_{TM})$ states by local hybridization at the interface within the d band model for understanding adsorption behaviors on the surface.[51,52] The ε_d values are evaluated by

$$\varepsilon_d = \frac{\int N_{2p_z}^{O_i}(\varepsilon)\varepsilon d\varepsilon}{\int N_{2p_z}^{O_i}(\varepsilon) d\varepsilon}$$

where $N_{2p_z}^{O_i}(\varepsilon)$ is the PDOS of $2p_z(O_i)$ states at the energy, ε, with respect to E_F.

In particular, the results for 3d TM, from Ti to Co, obtained from GGA calculations were ascertained again by semiempirical correction of on-site Coulomb interaction based on the Hubbard model,[53] which can improve the description of systems with strongly correlated d or f electrons. In this study, we employed the DFT+U approach suggested by S. L. Dudarev et al.[54] implemented in VASP. In this method, the on-site Coulomb interaction is simplified by the effective Hubbard *U* parameter, $U_{eff} = \bar{U} - \bar{J}$, where $\bar{U}$ and $\bar{J}$ are spherically averaged matrix elements of the screened Coulomb electron–electron interaction. The U_{eff} values and the computational results obtained by DFT+U methods are in Table S3 of the Supporting Information. The deviation in magnetic moments and atomic charges of impurity dopants obtained by DFT+U methods becomes larger as the number of unpaired 3d electrons increases (Figure S1 of the Supporting Information). However, the differences in the reaction energies coming from the correction by applying the Hubbard *U* parameter are not large, and thus the maximum deviation in the reaction energies is below 0.1 eV (Table S2 and Figure S6 of the Supporting Information). The minimum and maximum positions along the 3d TM series are, in particular, maintained in DFT+U calculation results. Therefore, our approach using DFT based on the GGA method is reasonable for examining relative change during chemical reactions on ultrathin oxide films grown on a TM-doped metal substrate.

ASSOCIATED CONTENT

Supporting Information

Numerical values regarding the stability of 3d transition metal (TM) dopants at the oxide–metal interface (i.e., formation energy); the numerical values of reaction energy for the dissociation of water molecules on bulk MgO(100), nondoped 1- and 2-ML MgO/Ag(100) and 2-ML MgO films supported by Ag(100) with O vacancy and 3d TM dopant at the oxide–metal interface; magnetic moments and atomic charges of 3d TM dopants during water dissociation on interface-doped MgO/Ag(100); charge density difference maps for 3d TM-doped and nondoped MgO/Ag(100) before adsorption of water molecules (**S**), after adsorption of water molecules (**A**), and at dissociative adsorption of water molecules (**D**); description of charge density redistribution at the oxide–metal interface during the dissociation of water molecules on the MgO/Ag(100) with an interface dopant; projected density of states (PDOS) diagrams regarding the electronic states of dopant and interface oxygen during water dissociation; effective Hubbard U parameters for 3d TM elements; reaction energies for the dissociation of individual water molecules on MgO/Ag(100) with interface dopant of 3d TM, obtained using both GGA and GGA+U methods. This material is available free of charge via the Internet at http://pubs.acs.org.

AUTHOR INFORMATION

Corresponding Author

*ykim@riken.jp, maki@k.u-tokyo.ac.jp

Notes

The authors declare no competing financial interest.

■ ACKNOWLEDGMENTS

This work was financially supported in part by a Grant-in-Aid for Scientific Research on Priority Areas "Electron Transport through a Linked Molecule in Nano-scale" and a Grant-in-Aid for Scientific Research(S) "Single Molecule Spectroscopy using Probe Microscope" from the Ministry of Education, Culture, Sports, Science, and Technology (MEXT), Japan, and in part by the Global COE Program (Chemistry Innovation through Cooperation of Science and Engineering), MEXT, Japan. We are grateful for the computational resources of the RIKEN Integrated Cluster of Clusters (RICC) supercomputer system. J.J. kindly acknowledges the International Program Associate (IPA) of RIKEN for financial support in his Ph.D. course. The authors thank N. Takagi, O. Sugino, M. Lippmaa and K. Terashima for fruitful discussion and suggestions. The authors also thank David W. Chapmon for carefully reading the manuscript.

■ REFERENCES

(1) Henrich, V. E.; Cox, P. A. *The Surface Science of Metal Oxides*; Cambridge University Press: Cambridge, 1994.
(2) Freund, H.-J. *Surf. Sci.* **2007**, *601*, 1438−1442.
(3) Diebold, U.; Li, S.-C.; Schmid, M. *Annu. Rev. Phys. Chem.* **2010**, *61*, 129−148.
(4) Nilius, N. *Surf. Sci. Rep.* **2009**, *64*, 595−659.
(5) Freund, H.-J. *Chem.—Eur. J.* **2010**, *16*, 9384−9397.
(6) Pacchioni, G.; Giordano, L.; Baistrocchi, M. *Phys. Rev. Lett.* **2005**, *94*, 226104.
(7) Sterrer, M.; Risse, T.; Pozzoni, U. M.; Giordano, L.; Heyde, M.; Rust, H.-P.; Pacchioni, G.; Freund, H.-J. *Phys. Rev. Lett.* **2007**, *98*, 096107.
(8) Ricci, D.; Bongiorno, A.; Pacchioni, G.; Landman, U. *Phys. Rev. Lett.* **2006**, *97*, 036106.
(9) Hellman, A.; Klacar, S.; Grönbeck, H. *J. Am. Chem. Soc.* **2009**, *131*, 16636−16637.
(10) Gonchar, A.; Risse, T.; Freund, H.-J.; Giordano, L.; Di Valentin, C.; Pacchioni, G. *Angew. Chem., Int. Ed.* **2011**, *50*, 2635−2638.
(11) Hellman, A.; Grönbeck, H. *Phys. Rev. Lett.* **2008**, *100*, 116801.
(12) Carrasco, E.; Brown, M. A.; Sterrer, M.; Freund, H.-J.; Kwapien, K.; Sierka, M.; Sauer, J. *J. Phys. Chem. C* **2010**, *114*, 18207−18214.
(13) Jung, J.; Shin, H.-J.; Kim, Y.; Kawai, M. *Phys. Rev. B* **2010**, *82*, 085413.
(14) Jung, J.; Shin, H.-J.; Kim, Y.; Kawai, M. *J. Am. Chem. Soc.* **2011**, *133*, 6142−6145.
(15) Shin, H.-J.; Jung, J.; Motobayashi, K.; Yanagisawa, S.; Morikawa, Y.; Kim, Y.; Kawai, M. *Nat. Mater.* **2010**, *9*, 442−447.
(16) Sun, Y.-N.; Qin, Z.-H.; Lewandowski, M.; Carrasco, E.; Sterrer, M.; Shaikhutdinov, S.; Freund, H.-J. *J. Catal.* **2009**, *266*, 359−368.
(17) Sun, Y.-N.; Giordano, L.; Goniakowski, J.; Lewandowski, M.; Qin, Z.-H.; Noguera, C.; Shaikhutdinov, S.; Pacchioni, G.; Freund, H.-J. *Angew. Chem., Int. Ed.* **2010**, *49*, 4418−4421.
(18) Altieri, S.; Contri, S. F.; Valeri, S. *Phys. Rev. B* **2007**, *76*, 205413.
(19) Holladay, J. D.; Hu, J.; King, D. L.; Wang, Y. *Catal. Today* **2009**, *139*, 244−260.
(20) Brown, G. E. J.; Henrich, V. E.; Casey, W. H.; Clark, D. L.; Eggleston, C.; Felmy, A.; Goodman, D. W.; Grätzel, M.; Maciel, G.; McCarthy, M. I.; Nealson, K. H.; Sverjensky, D. A.; Toney, M. F.; Zachara, J. M. *Chem. Rev.* **1999**, *99*, 77−174.
(21) Ponec, V. *Adv. Catal.* **1983**, *32*, 149−214.
(22) Besenbacher, F.; Chorkendorff, I.; Clausen, B. S.; Hammer, B.; Molenbroek, A. M.; Nørskov, J. K.; Stensgaard, I. *Science* **1998**, *279*, 1913−1915.
(23) Chen, M.; Kumar, D.; Yi, C.-W.; Goodman, D. W. *Science* **2005**, *310*, 291−293.
(24) Ulrich, S.; Nilius, N.; Freund, H.-J.; Martinez, U.; Giordano, L.; Pacchioni, G. *Phys. Rev. Lett.* **2009**, *102*, 016102.
(25) Griffith, J. S.; Orgel, L. E. *Q. Rev. Chem. Soc.* **1957**, *11*, 381−393.
(26) Matsumoto, Y.; Kurimoto, J.; Shimizu, T.; Sato, E. *J. Electrochem. Soc.* **1981**, *128*, 1040−1044.
(27) Matsumoto, Y.; Murakami, M.; Shono, T.; Hasegawa, T.; Fukumura, T.; Kawasaki, M.; Ahmet, P.; Chikyow, T.; Koshihara, S.; Koinuma, H. *Science* **2001**, *291*, 854−856.
(28) Shao, X.; Prada, S.; Giordano, L.; Pacchioni, G.; Nilius, N.; Freund, H.-J. *Angew. Chem., Int. Ed.* **2011**, *50*, 11525−11527.
(29) Shao, X.; Nilius, N.; Freund, H.-J. *J. Am. Chem. Soc.* **2012**, *134*, 2532−2534.
(30) Madsen, G. K. H.; Hammer, B. *J. Chem. Phys.* **2009**, *130*, 044704.
(31) Sander, D. *Curr. Opin. Solid State Mater. Sci.* **2003**, *7*, 51−57.
(32) Toulhoat, H.; Raybaud, P. *J. Catal.* **2003**, *216*, 63−72.
(33) Ruban, A. V.; Skriver, H. L.; Nørskov, J. K. *Phys. Rev. B* **1999**, *59*, 15990−16000.
(34) Patthey, F.; Massobrio, C.; Schneider, W.-D. *Phys. Rev. B* **1996**, *53*, 13146−13149.
(35) Figgis, B. N. *Introduction to Ligand Fields*; Interscience: New York, 1966.
(36) Johnson, D. A.; Nelson, P. G. *Inorg. Chem.* **1995**, *34*, 5666−5671.
(37) Jarvis, E. A. A.; Carter, E. A. *J. Phys. Chem. B* **2002**, *106*, 7995−8004.
(38) Pacchioni, G. *Surf. Sci.* **2002**, *520*, 3−5.
(39) Goniakowski, J.; Noguera, C. *Interface Sci.* **2004**, *12*, 93−103.
(40) Hammer, B.; Nørskov, J. K. *Nature* **1995**, *376*, 238−240.
(41) Ohtomo, A.; Muller, D. A.; Grazul, J. L.; Hwang, H. Y. *Nature* **2002**, *419*, 378−380.
(42) Yuasa, S.; Nagahama, T.; Fukushima, A.; Suzuki, Y.; Ando, K. *Nat. Mater.* **2004**, *3*, 868−871.
(43) Kresse, G.; Hafner, J. *Phys. Rev. B* **1993**, *47*, 558−561.
(44) Kresse, G.; Furthmüller, J. *Phys. Rev. B* **1996**, *54*, 11169−11186.
(45) Perdew, J. P.; Wang, Y. *Phys. Rev. B* **1992**, *45*, 13244−13249.
(46) Perdew, J. P.; Chevary, J. A.; Vosko, S. H.; Jackson, K. A.; Pederson, M. R.; Singh, D. J.; Fiolhais, C. *Phys. Rev. B* **1992**, *46*, 6671−6687.
(47) Kresse, G.; Joubert, D. *Phys. Rev. B* **1999**, *59*, 1758−1775.
(48) Prada, S.; Martinez, U.; Pacchioni, G. *Phys. Rev. B* **2008**, *78*, 235423.
(49) Tang, W.; Sanville, E.; Henkelman, G. *J. Phys.: Condens. Matter* **2009**, *21*, 084204.
(50) Henkelman, G.; Uberuaga, B. P.; Jónsson, H. *J. Chem. Phys.* **2000**, *113*, 9901−9904.
(51) Hammer, B.; Nørskov, J. K. *Adv. Catal.* **2000**, *45*, 71−129.
(52) Nørskov, J. K.; Bligaard, T.; Rossmeisl, J.; Christensen, C. H. *Nature Chem.* **2009**, *1*, 37−46.
(53) Anisimov, V. I.; Korotin, M. A.; Kurmaev, E. Z. *J. Phys.: Condens. Matter* **1990**, *2*, 3973−3987.
(54) Dudarev, S. L.; Botton, G. A.; Savrasov, S. Y.; Humphreys, C. J.; Sutton, A. P. *Phys. Rev. B* **1998**, *57*, 1505−1509.